


## Article

# The Enhanced Performance of NiCuOOH/NiCu(OH)<sub>2</sub> Electrode Using Pre-Conversion Treatment for the Electrochemical Oxidation of Ammonia

Xuejiao Yin <sup>1,\*</sup>, Jiabin Wen <sup>1</sup>, Jujiao Zhao <sup>2</sup> , Ran An <sup>2</sup>, Ruolan Zhang <sup>2</sup>, Yin Xiong <sup>3</sup>, Yanzong Tao <sup>3</sup>, Lingxin Wang <sup>4</sup>, Yuhang Liu <sup>4</sup>, Huanyu Zhou <sup>5</sup> and Yuanyuan Huang <sup>6,7,\*</sup>

<sup>1</sup> School of Architecture and Engineering, Chongqing Industry Polytechnic College, Chongqing 401120, China

<sup>2</sup> College of Environment and Resources, Chongqing Technology and Business University, Chongqing 400067, China; zhaojujiao@ctbu.edu.cn (J.Z.)

<sup>3</sup> Chongqing Baihan Wastewater Treatment Co., Ltd., Chongqing 400000, China; 13594739722@163.com (Y.X.)

<sup>4</sup> School of Civil Engineering and Architecture, Chongqing University of Science and Technology, Chongqing 401331, China

<sup>5</sup> Green Intelligence Environmental School, Yangtze Normal University, Chongqing 408100, China

<sup>6</sup> Key Laboratory of Hydraulic and Waterway Engineering of the Ministry of Education, School of River and Ocean Engineering, Chongqing Jiaotong University, Chongqing 400074, China

<sup>7</sup> Chongqing Academy of Science and Technology, Chongqing 401120, China

\* Correspondence: yinxuejiao1012@126.com (X.Y.); 18983093831@163.com (Y.H.)

**Abstract:** Electrochemical oxidation of ammonia is an attractive process for wastewater treatment, hydrogen production, and ammonia fuel cells. However, the sluggish kinetics of the anode reaction has limited its applications, leading to a high demand for novel electrocatalysts. Herein, the electrode with the in situ growth of NiCu(OH)<sub>2</sub> was partially transformed into the NiCuOOH phase by a pre-treatment using highly oxidative solutions. As revealed by SEM, XPS, and electrochemical analysis, such a strategy maintained the 3D structure, while inducing more active sites before the in situ generation of oxyhydroxide sites during the electrochemical reaction. The optimized NiCuOOH-1 sample exhibited the current density of 6.06 mA cm<sup>-2</sup> at 0.5 V, which is 1.67 times higher than that of NiCu(OH)<sub>2</sub> (3.63 mA cm<sup>-2</sup>). Moreover, the sample with a higher crystalline degree of the NiCuOOH phase exhibited lower performance, demonstrating the importance of a moderate treatment condition. In addition, the NiCuOOH-1 sample presented low selectivity (<20%) towards NO<sub>2</sub><sup>-</sup> and stable activity during the long-term operation. The findings of this study would provide valuable insights into the development of transition metal electrocatalysts for ammonia oxidation.

**Keywords:** electrochemical oxidation of ammonia; nickel–copper oxyhydroxide; wastewater treatment; hydrogen production



**Citation:** Yin, X.; Wen, J.; Zhao, J.; An, R.; Zhang, R.; Xiong, Y.; Tao, Y.; Wang, L.; Liu, Y.; Zhou, H.; et al. The Enhanced Performance of NiCuOOH/NiCu(OH)<sub>2</sub> Electrode Using Pre-Conversion Treatment for the Electrochemical Oxidation of Ammonia. *Molecules* **2024**, *29*, 2339. <https://doi.org/10.3390/molecules29102339>

Academic Editor: Antonella Curulli

Received: 1 April 2024

Revised: 9 May 2024

Accepted: 13 May 2024

Published: 16 May 2024



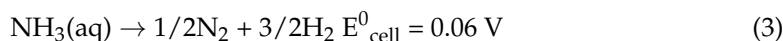
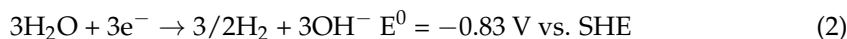
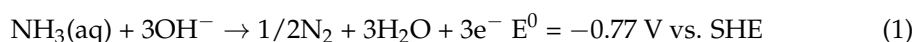
**Copyright:** © 2024 by the authors. Licensee MDPI, Basel, Switzerland. This article is an open access article distributed under the terms and conditions of the Creative Commons Attribution (CC BY) license (<https://creativecommons.org/licenses/by/4.0/>).

## 1. Introduction

Ammonia, a compound synthesized in vast quantities for fertilizers, industrial processes, and various agricultural activities, has inadvertently become a severe environmental hazard [1–3]. Excess ammonia in wastewater can precipitate a host of environmental problems, notably eutrophication. This phenomenon, characterized by an overgrowth of algae due to high nutrient concentrations, disrupts aquatic ecosystems and significantly deteriorates water quality [4]. Moreover, a high concentration of ammonia can act as an irritant and cause severe damage to the respiratory tract, eyes, and skin [5]. Thus, tackling the issue of ammonia pollution is an environmental imperative that demands immediate and innovative solutions.

Against this backdrop, the electrochemical oxidation of ammonia has emerged as a promising avenue for its degradation [3,6,7]. More importantly, this process has the added advantage of simultaneously generating hydrogen, a clean and renewable energy carrier [2].

This dual benefit renders the electrochemical oxidation of ammonia to be an appealing strategy in the broader context of sustainable energy and environmental conservation. The overall reaction is defined as follows [8,9]:



One of the attractive aspects of this reaction is that it can occur at a surprisingly low potential of just 0.06 V, an attribute that makes this process energy-efficient and potentially economically feasible [10]. Nevertheless, the efficiency and practical applicability of the electrochemical oxidation of ammonia largely hinge upon the choice and design of the catalyst involved [10]. Traditionally, catalysts for this process have relied heavily on noble metals [11]. The overpotential of Pt for the electrochemical oxidation of ammonia is approximately 0.48 V; thus, Pt has been regarded as the most effective ammonia oxidation electrocatalyst for an extended period [12]. Nevertheless, Pt undergoes fast deactivation during the electrochemical oxidation of ammonia since the binding energy of N atoms on the Pt surface is too strong, impeding its practical applications. To overcome this demerit, some Pt-based complexes such as PtRh/C [13] and PtSnO<sub>2</sub>/C [8] have been developed. Although the stability of these catalysts has been improved, the high cost and scarcity of noble metals still seriously impede their large-scale applications, motivating the quest for cost-effective alternatives [14–16].

Research on non-noble metals and their compounds has been pursued as an avenue to circumvent these challenges. Nickel-based catalysts have shown some promise due to their abundance, low cost, and reasonable activity [17–21]. Recently, it is widely reported that the NiCu-based bi-metal catalysts show better activity than other bi-metal catalysts and single-metal catalysts, suggesting its potential for applications [6,22–29]. However, the performance of these materials still needs to be improved.

It is presumed by several studies that the actual active phase of the NiCu-based catalysts is the NiCu oxyhydroxide phase (NiCuOOH), which is formed in situ during the electrochemical reaction [17,21,27,30]. The formation of NiCuOOH under anodic conditions has been regarded as the key step before the electrochemical oxidation of ammonia. This improvement is largely attributed to the unique electronic structure and greater availability of active sites in the NiCuOOH phase [22,31].

Yet, the inherent challenge with such catalysts lies in the fact that the NiCu atoms on the surface of electrode might not be totally converted into the NiCuOOH phase in the electrochemical oxidation process. Compared to the pure NiCuOOH phase, the amount of in situ-generated NiCuOOH active sites might be limited, potentially constraining the performance of these catalysts. Furthermore, the in situ-formed NiCuOOH generally exhibited low crystallinity. Despite some studies reporting that the non-crystalline materials exhibit better electrochemical activity [32], very few studies have assessed the influence of the crystalline degree for the electrochemical oxidation of ammonia.

According to the current insights in this field, it seems that a pure NiCuOOH electrode should be a better choice than other NiCu-based electrocatalysts. However, the NiCuOOH electrode did not exhibit superior performance than other electrodes [22,27]. One of the main reasons is that the morphology of NiCuOOH is difficult to adjust. It is well known that the morphology of catalysts plays an important role in the electrochemical reaction [33]. The 3D nanostructure of catalysts could contribute to their effectiveness by ensuring a high surface area and shorter diffusion paths. These nanostructures enhance reactant access to active sites and product removal, thereby accelerating the overall reaction rate [34].

Thus, based on all above facts, the  $\text{NiCu}(\text{OH})_2$  electrode with a well-defined 3D structure was synthesized, and it was treated by a pre-treatment before the electrochemical reaction to form the 3D  $\text{NiCuOOH}$  phase with different crystalline degrees. The pre-treatment process partially transforms the  $\text{NiCu}(\text{OH})_2$  into the active phase  $\text{NiCuOOH}$  while preserving the beneficial 3D nanostructure. This approach has led to a significant improvement in catalyst performance, being a major step forward in the practical application of these materials for the electrochemical oxidation of ammonia.

## 2. Results and Discussion

### 2.1. Characterization of Catalysts

The crystalline structures of the prepared samples were investigated using XRD, and the obtained patterns are presented in Figure 1. For the as-prepared  $\text{NiCu}(\text{OH})_2$  sample, the observed XRD pattern shows characteristic peaks located at  $16.7^\circ$ ,  $32.4^\circ$ , and  $39.8^\circ$ , which correspond to the reported  $\text{NiCu}(\text{OH})_2$ , indicating its successful synthesis [24]. In the pattern of the  $\text{NiCuOOH-1}$  sample, the intensity of the peak located at around  $16.7^\circ$  corresponding to the (020) facet of  $\text{Cu}(\text{OH})_2$  (JCPDS no. 13-0420) significantly decreased. All the other peaks belonging to  $\text{NiCu}(\text{OH})_2$  also present lower intensity. Meanwhile, the peaks corresponding to the (002) facet of  $\text{NiCuOOH}$  could be observed [35,36], demonstrating the partial transformation of  $\text{NiCu}(\text{OH})_2$  into  $\text{NiCuOOH}$  as a result of our pre-treatment process. The XRD pattern of the  $\text{NiCuOOH-2}$  sample, which is prepared by a higher concentration of  $\text{KOH}$  and  $\text{K}_2\text{S}_2\text{O}_8$ , was also collected, and it shows peaks exclusively matching the  $\text{NiCuOOH}$  phase. These results illustrate the impact of the pre-treatment process on the phase transformation of  $\text{NiCu}(\text{OH})_2$  into  $\text{NiCuOOH}$  and indicate that the  $\text{NiCuOOH}$  phase was successfully formed after the pre-treatment process.

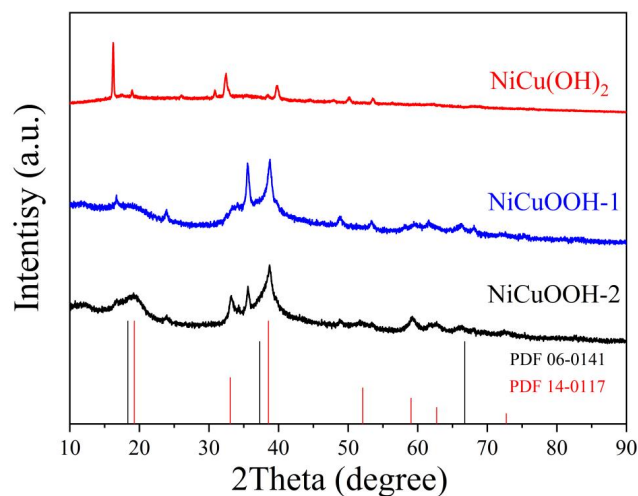


**Figure 1.** The XRD patterns of  $\text{NiCu}(\text{OH})_2$ ,  $\text{NiCuOOH-1}$ , and  $\text{NiCuOOH-2}$ .

The morphology of the samples was observed by SEM (Figure 2). The SEM image (Figure 2a) of  $\text{NiCu}(\text{OH})_2$  clearly reveals the porous nanostructure consisting of overlapped nanorods, which is similar to that of reported studies [24]. Interestingly, the SEM images of the pre-treated samples,  $\text{NiCuOOH-1}$  and  $\text{NiCuOOH-2}$ , also exhibit a similar nanostructure. Despite the phase transformation from  $\text{NiCu}(\text{OH})_2$  to  $\text{NiCuOOH}$  that occurs during the pre-treatment process, the overall morphology of the samples appears to be largely unchanged.

To further investigate the microstructure of the samples, TEM was conducted, and the images are depicted in Figure 3. The powder of each sample was stripped from the carbon cloth by the ultrasonic treatment used for the TEM measurement. It could be noticed that  $\text{NiCuOOH-1}$  and  $\text{NiCuOOH-2}$  also present a similar nanostructure, further indicating that the pre-treatment process did not change the morphology of these samples.

The length of these nanorods is approximately 100 to 300 nm; meanwhile, their width is approximately 20 to 50 nm. Based on the XRD, SEM, and TEM results, it is suggested that the pre-treatment method successfully induces the phase transformation while preserving the beneficial nanostructure.

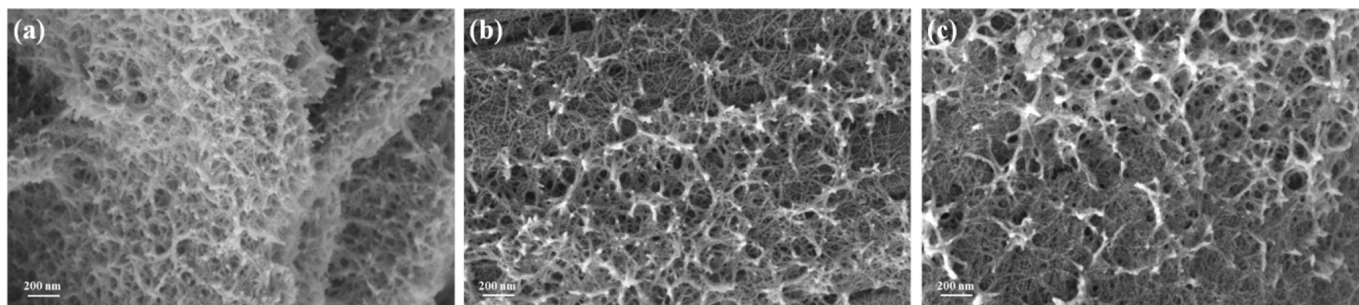


**Figure 2.** (a) The SEM image of  $\text{NiCu}(\text{OH})_2$ , (b) the SEM image of  $\text{NiCuOOH-1}$ , and (c) the SEM image of  $\text{NiCuOOH-2}$ .

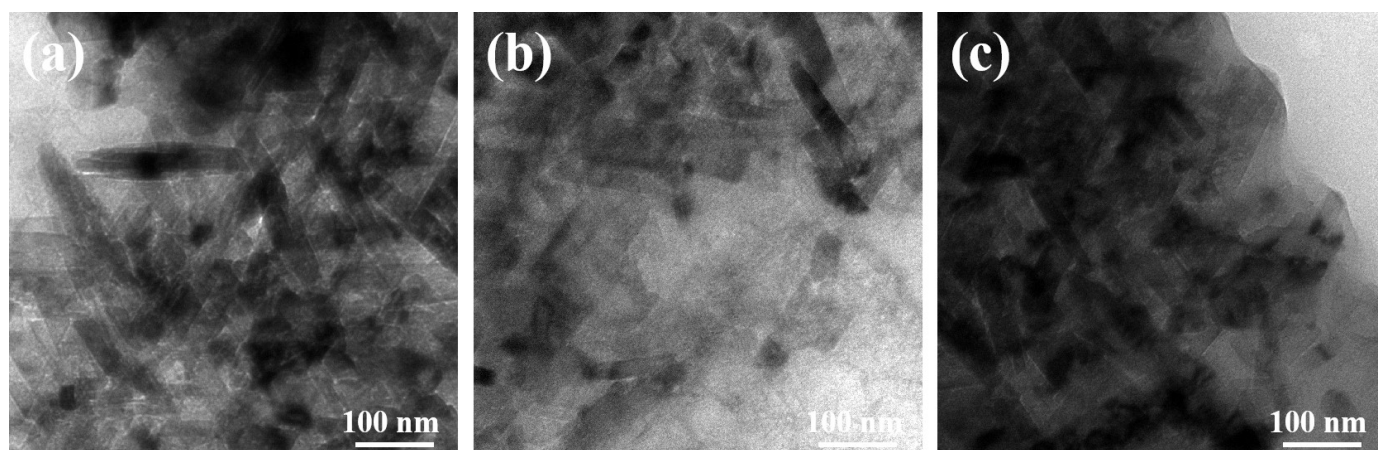


**Figure 3.** (a) The TEM image of  $\text{NiCu}(\text{OH})_2$ , (b) the TEM image of  $\text{NiCuOOH-1}$ , and (c) the TEM image of  $\text{NiCuOOH-2}$ .

The surface composition and chemical states of the prepared samples were investigated using XPS. The XPS survey spectra (Figure S1) confirmed the presence of Ni, Cu, and O in all three samples, without any noticeable impurities. The high-resolution spectra of  $\text{Cu } 2p_{3/2}$  with the peak located at  $934.5 \pm 0.3 \text{ eV}$  could be ascribed to the presence of  $\text{Cu}(\text{II})$  [23,37]. All the three samples showed similar spectra, as shown in Figures 4a and S2. For the high-resolution Ni spectrum of the  $\text{NiCu}(\text{OH})_2$  sample (Figure 4b), peaks at 856.4 and 862.0 eV corresponding to  $\text{Ni } 2p_{3/2}$  and its satellite peak of  $\beta\text{-Ni}(\text{OH})_2$  could be observed [18,23], which is in accordance with the XRD results. In the  $\text{NiCuOOH-1}$  sample, the  $\text{Ni } 2p_{3/2}$  showed the presence of both  $\text{Ni}^{\text{II}}$  and  $\text{Ni}^{\text{III}}$ , indicating the partial transformation of  $\text{NiCu}(\text{OH})_2$  to the  $\text{NiCuOOH}$  phase during the pre-treatment [18,38,39].  $\text{NiCuOOH-2}$ , the sample treated with a solution having stronger oxidizing properties, presented the  $\text{Ni}^{\text{III}}/\text{Ni}^{\text{II}}$  value of 3.06; meanwhile, the  $\text{Ni}^{\text{III}}/\text{Ni}^{\text{II}}$  value of  $\text{NiCuOOH-1}$  is just 0.62, indicating the increased amount of  $\text{Ni}^{\text{III}}$  on the surface of  $\text{NiCuOOH-2}$ .

Based on the XRD and XPS results, it could be concluded that the pre-treatment process reported in this study could successfully transform  $\text{NiCu}(\text{OH})_2$  into the  $\text{NiCuOOH}$  phase, and the crystalline degree can be adjusted.

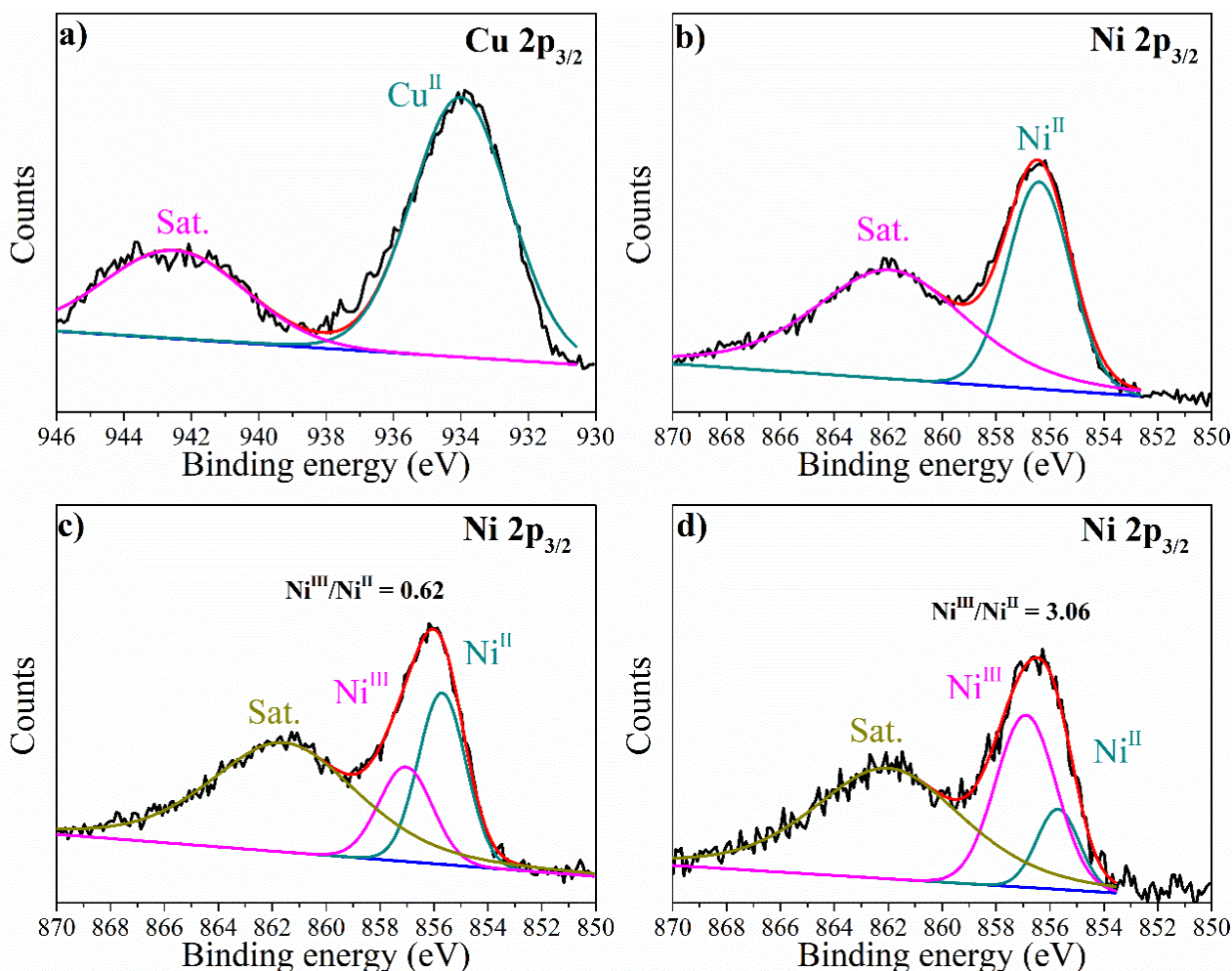


**Figure 4.** The high-resolution XPS spectra of (a) Cu  $2p_{3/2}$  of NiCuOOH-1, (b) Ni  $2p_{3/2}$  of NiCu(OH)<sub>2</sub>, (c) Ni  $2p_{3/2}$  of NiCuOOH-1, and (d) Ni  $2p_{3/2}$  of NiCuOOH-2.

## 2.2. Electrochemical Performance of Samples

The NiCu(OH)<sub>2</sub> with different Ni:Cu ratios was evaluated by LSV, and the 8:2 sample presented the best performance (Figure S3), which is in agreement with the results reported by other studies [22,24,26]. The electrochemical activity of NiCu(OH)<sub>2</sub>, NiCuOOH-1, and NiCuOOH-2 towards the oxidation of ammonia was first investigated using LSV, as shown in Figure S4a. In the electrolyte containing 0.1 mol/L KOH and 0.1 mol/L NH<sub>3</sub>, all the three samples presented a larger current density than those in the 0.1 mol/L KOH, indicating their activity towards the electrochemical oxidation of ammonia. The onset potentials of the three samples are all around 0.38–0.4 V (the potential with the current density of 1 mA cm<sup>-2</sup> was treated as the onset potential). Both NiCuOOH-1 and NiCuOOH-2 present the oxidation peak after the onset potential in the solution without 0.1 mol/L NH<sub>3</sub>, and the current density decreases with the increase in potential in this pure KOH solution until the potential is higher than 0.53 V. These peaks could be attributed to the oxidation of Ni and/or Cu on the electrode, which is also reported by other studies [22]. Since the amount of Ni and Cu on the electrode is limited, the current density decreased even with a higher potential in the potential range without other chemical reactions. The increase in current density after 0.53 V could be due to water electrolysis. With the presence of NH<sub>3</sub>, the current densities of NiCuOOH-1 and NiCuOOH-2 increase in a linear manner when the potential is higher than 0.38 V. These results indicate that the oxidation of ammonia in this potential range. It can be noticed that NiCuOOH-1 presented better activity than NiCuOOH-2 for ammonia electrolysis; meanwhile, their performance for water electrolysis

is quite similar. They exhibited significantly larger current density than  $\text{NiCu}(\text{OH})_2$  for both water electrolysis and ammonia electrolysis. For investigating the kinetics of these samples for the electrochemical oxidation of ammonia, Tafel slopes were calculated, as shown in Figure S4b. The Tafel slope values of  $\text{NiCu}(\text{OH})_2$ ,  $\text{NiCuOOH-1}$ , and  $\text{NiCuOOH-2}$  are 151, 76, and 110  $\text{mV decade}^{-1}$ , respectively. The  $\text{NiCuOOH-1}$  presents the smallest Tafel slope value (76  $\text{mV decade}^{-1}$ ), indicating its faster reaction kinetics compared to those of  $\text{NiCu}(\text{OH})_2$  and  $\text{NiCuOOH-2}$ .

To further reveal the performance of three samples for the electrochemical oxidation of ammonia, chronoamperogram at different potentials was obtained (Figure 5). By maintaining the working voltage for a relatively long time, the current obtained in the chronoamperogram tests is close to the actual performance of the samples. The current density values obtained in 0.1 mol/L KOH with 0.1 mol/L  $\text{NH}_3$  minus those obtained in only 0.1 mol/L KOH were regarded as the response current density towards electrochemical oxidation of ammonia, and the current efficiency was calculated by dividing the response current density by the current density obtained in 0.1 mol/L KOH with 0.1 mol/L  $\text{NH}_3$ . For all the samples, the response current density increased when the working potential increased from 0.4 V to 0.6 V. At 0.4 V, the response current densities of  $\text{NiCu}(\text{OH})_2$ ,  $\text{NiCuOOH-1}$ , and  $\text{NiCuOOH-2}$  are 0.30, 1.02, and 0.56  $\text{mA cm}^{-2}$ , respectively, indicating the better performance of  $\text{NiCuOOH-1}$  under this voltage. Notably,  $\text{NiCuOOH-1}$  exhibited the response current density of 6.06  $\text{mA cm}^{-2}$  towards ammonia oxidation at 0.5 V, while its value for  $\text{NiCu}(\text{OH})_2$  is just 3.63  $\text{mA cm}^{-2}$ . Although the current efficiency of  $\text{NiCuOOH-1}$  for ammonia oxidation is 87.9%, which is slightly lower than that of  $\text{NiCu}(\text{OH})_2$  (96.8%), a much higher response current density indicates that  $\text{NiCuOOH-1}$  shows better performance than  $\text{NiCu}(\text{OH})_2$ . However,  $\text{NiCuOOH-2}$ , which exhibited a higher crystalline degree, presented a response current density of just 3.68  $\text{mA cm}^{-2}$  and current efficiency of just 83.6% at 0.5 V, both of which are lower than those of  $\text{NiCuOOH-1}$ . By further increasing the crystalline degree of samples resulted in worse activity, demonstrating that a moderate treatment condition is necessary for improving the performance.

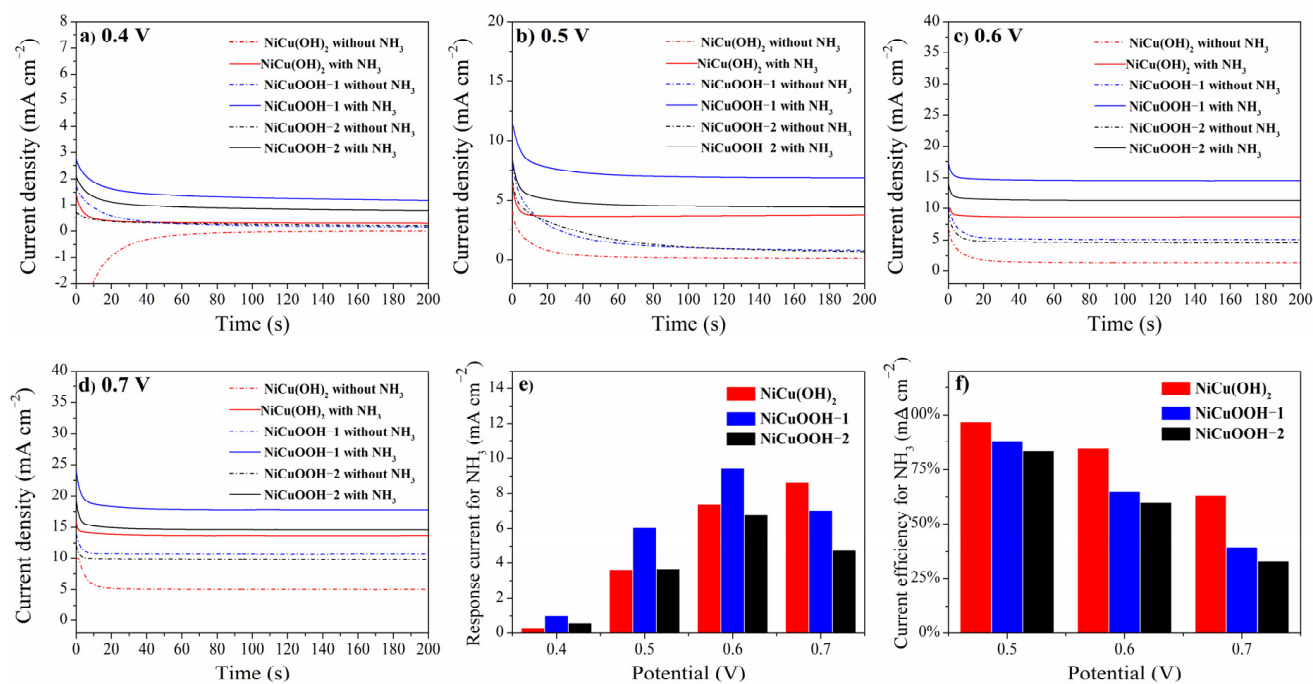


**Figure 5.** (a–d) Chronoamperogram of three samples at 0.4 V, 0.5 V, 0.6 V, and 0.7 V, respectively, in 0.1 mol/L KOH with or without 0.1 mol/L  $\text{NH}_3$  and (e,f) the calculated response current towards ammonia and the current efficiency for ammonia oxidation.

Further increasing the working potentials to 0.6 V, a response current density of  $9.45 \text{ mA cm}^{-2}$  could be obtained on NiCuOOH-1, which is also higher than those of NiCu(OH)<sub>2</sub> ( $7.37 \text{ mA cm}^{-2}$ ) and NiCuOOH-1 ( $6.78 \text{ mA cm}^{-2}$ ). However, current efficiency significantly decreased to 65.0%. At 0.7 V, the current efficiency of NiCuOOH-1 further decreased to 40.0%; meanwhile, the response current density also decreased to  $7.02 \text{ mA cm}^{-2}$ . This could be attributed to the enhanced oxygen evolution reaction at high working potentials, in accordance with the reported studies [29,30]. Thus, based on the results shown above, 0.5 V was suggested to be used as the optimized working potential in the following experiments.

To further evaluate the performance of NiCuOOH-1, chronoamperogram were conducted at 0.5 V with different ammonia concentrations. As shown in Figure 6a, the current density increased by increasing the ammonia concentration, further indicating that the increased current originates from the electrochemical oxidation of ammonia. By increasing the ammonia concentration from 0.02 mol/L to 0.05 mol/L, the current density increased from  $2.79 \text{ mA cm}^{-2}$  to  $4.86 \text{ mA cm}^{-2}$ . However, it could be noticed that the current density for 0.5 mol/L ammonia is just slightly higher than that for 0.2 mol/L ammonia, which could be attributed to the limited ammonia diffusion in the solution [17].

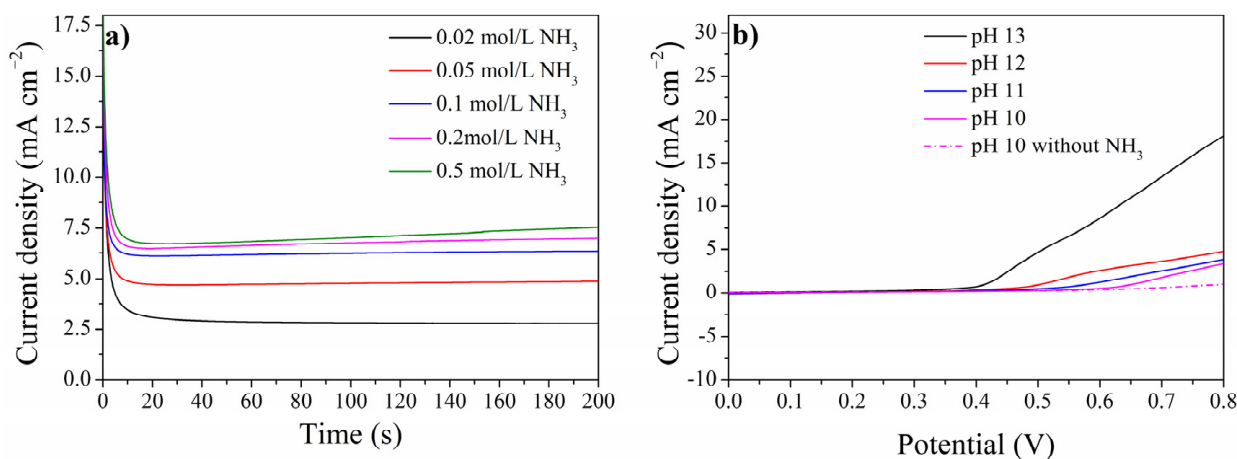


**Figure 6.** (a) Chronoamperogram of NiCuOOH-1 with different ammonia concentrations at 0.5 V and (b) the LSV curves of NiCuOOH-1 at different pHs.

The performance of NiCuOOH-1 at different pH values was also tested, as shown in Figure 6b. Even at pH 10, the NiCuOOH-1 exhibited an obvious response current for ammonia oxidation. Despite NiCuOOH-1 showing activity in the pH range of 10 to 14, it could be noticed that the pH significantly affects the performance of NiCuOOH-1. The observed current density at 0.7 V decreased from  $13.42 \text{ mA cm}^{-2}$  (pH 13) to  $3.64 \text{ mA cm}^{-2}$  (pH 12). As shown in Equation (1), the oxidation of ammonia on anode needs the participation of OH<sup>-</sup>. The higher activity at a higher pH indicates the key role of OH<sup>-</sup> in the electrochemical oxidation of ammonia, as reported by other studies [7,40].

### 2.3. Ammonia Electrolisis at Different Voltages

The selectivity of electrochemical oxidation of ammonia is very important since NO<sub>2</sub><sup>-</sup> and NO<sub>3</sub><sup>-</sup> are still regarded as pollutants that could be harmful to human health and the environment. The removal of NH<sub>3</sub> with NiCuOOH-1 as the working electrode in a two-chamber reactor was conducted at 0.5 V, 0.6 V, and 0.7 V, respectively. The ammonia removal with a NiCu(OH)<sub>2</sub> electrode was also evaluated at 0.5 V as the counter experiment to reveal the performance of NiCuOOH-1. The initial concentration of NH<sub>3</sub> is 0.1 mol/L (1400 mg/L N). As depicted in Figure 7a, within 8 h, 38.02% of NH<sub>3</sub> could be removed at 0.5 V by NiCuOOH-1, while 28.26% can be removed by NiCu(OH)<sub>2</sub>, further indicating the better performance of NiCuOOH-1. The NH<sub>3</sub> removal rate of NiCuOOH-1 at 0.6 V

and 0.7 V within 8 h is 52.08% and 69.05%, respectively. The  $\text{NH}_3$  removal rate increases when the applied voltage is higher, which is in agreement with the increased response current for  $\text{NH}_3$  at these voltages. In all the experiments, the concentration of  $\text{NO}_3^-$  within 8 h is less than 5 mg/L, which can be ignored. However, the accumulation of  $\text{NO}_2^-$  is observed, as shown in Figure 7b. The conversion rate from  $\text{NH}_3$  to  $\text{NO}_2^-$  of NiCuOOH-1 at 0.5 V, 0.6 V, and 0.7 V is 16.72%, 17.43%, and 18.22%, respectively. Despite the slight increase in the conversion rate, NiCuOOH-1 exhibits low  $\text{NO}_2^-$  selectivity of less than 20.00% in the voltage range of 0.5 V to 0.7 V, implying its potential for being utilized in wastewater treatment.

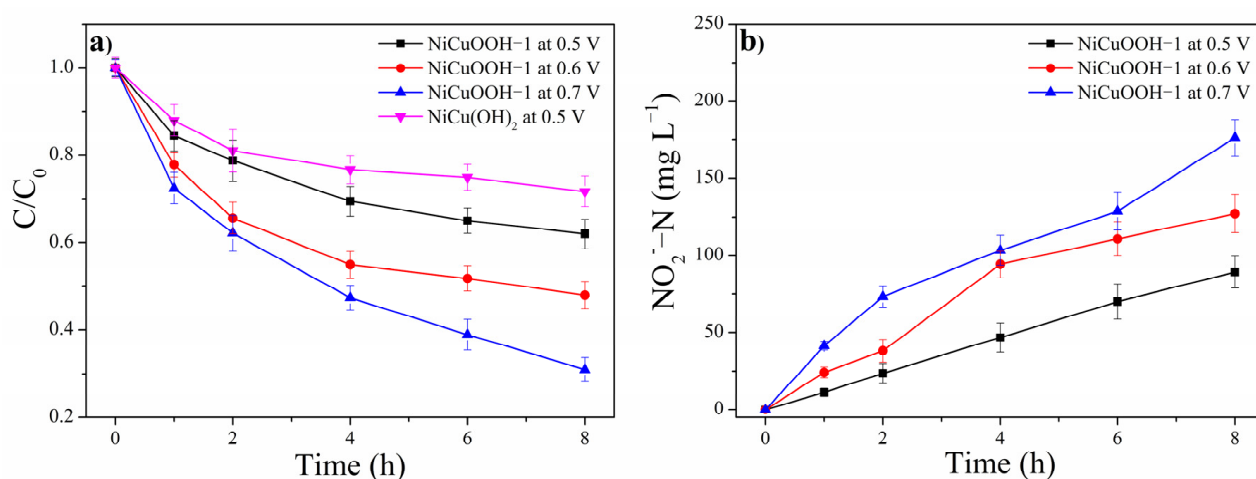


**Figure 7.** (a)  $\text{NH}_3$  removal in a two-chamber reactor by NiCuOOH-1 and NiCu(OH)<sub>2</sub> at different voltages with an initial  $\text{NH}_3$  concentration of 0.1 mol/L and (b) the generation of  $\text{NO}_2^-$  by NiCuOOH-1 at different voltages.

#### 2.4. Mechanism Investigation

The origin of the good performance of NiCuOOH-1 was further investigated. It is known that the electrochemical surface area (ECSA) plays an important role in the electrochemical reaction, and it has a proportional correlation with the double-layer capacitance (Cdl) [10]. Thus, the Cdl values of NiCu(OH)<sub>2</sub>, NiCuOOH-1, and NiCuOOH-2 were extracted from CV measurements taken at various scan rates in a potential range where no Faradaic reactions occur, as depicted in Figure 8. The Cdl values of NiCu(OH)<sub>2</sub>, NiCuOOH-1, and NiCuOOH-2 were 8.7, 12.0, and 12.6 mF cm<sup>-2</sup>, respectively. The partial pre-transformation from NiCu(OH)<sub>2</sub> to the NiCuOOH phase significantly improved the Cdl, indicating that NiCuOOH-1 exhibited a larger ECSA than NiCu(OH)<sub>2</sub>. In other words, NiCuOOH-1 has more electrochemical active sites than NiCu(OH)<sub>2</sub>. The NiCuOOH-2 samples, which are treated under a higher oxidation condition, showed similar Cdl compared to NiCuOOH-1. This result suggested that, although the higher oxidation treatment could further improve the crystalline degree, it might not increase the amount of oxyhydroxide sites on the surface. Taking the better performance of NiCuOOH-1 into consideration, these results indicate that the better performance of NiCuOOH-1 could be due to the larger ECSA, which might originate from the partial transformation of NiCu(OH)<sub>2</sub> into the NiCuOOH phase.



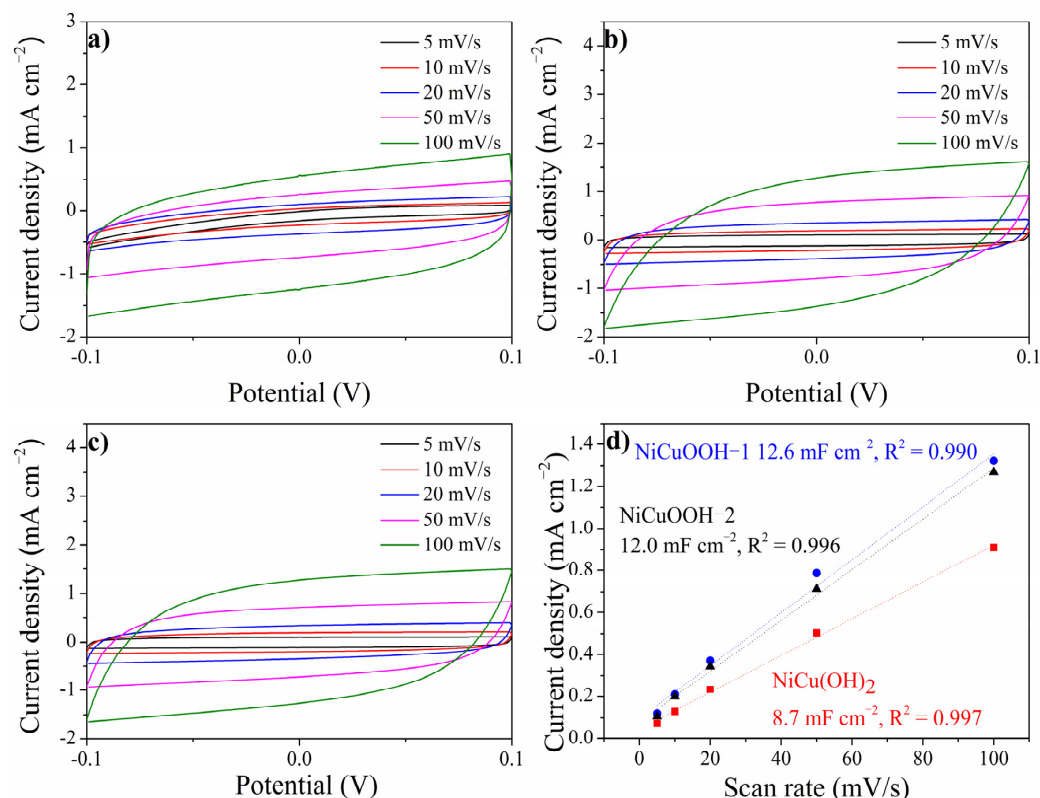


**Figure 8.** (a–c) CV measurements at different scan rates (5, 10, 20, 50, and 100 mV/s) of NiCu(OH)<sub>2</sub>, NiCuOOH-1, and NiCuOOH-2, respectively, and (d) the calculated C<sub>dl</sub> values.

### 2.5. Stability of NiCuOOH-1

The stability of electrocatalysts is an important factor for potential practical applications. Hence, the long-term operation by NiCuOOH-1 was conducted. The chronoamperogram of NiCuOOH-1 was performed at 0.5 V for 1.5 h in 0.1 mol/L NH<sub>3</sub>. After that, the solution was replaced to exclude the influence of the change in the ammonia concentration, and the LSV curve was recorded in the fresh solution containing 0.1 mol/L NH<sub>3</sub>. Then, the same NiCuOOH-1 sample was tested for another 1.5 h. As shown in Figure 9, after 10 cycles (15 h of continuous operation), no attenuation could be observed in the recorded LSV curves. The SEM images of the NiCuOOH-1 sample after long-term operation is shown in Figure S5, and the sample retained the similar 3D structure. These results demonstrated the good stability of NiCuOOH-1 in the electrochemical oxidation of ammonia.

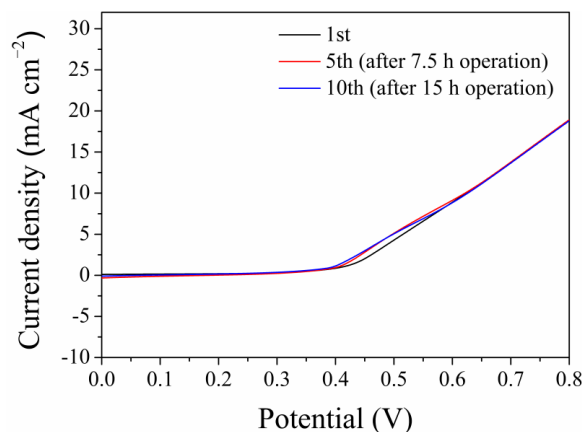


**Figure 9.** The stability tests of NiCuOOH-1. Each LSV was obtained for the same NiCuOOH-1 sample in fresh 0.1 mol/L KOH + 0.1 mol/L NH<sub>3</sub>.

### 3. Materials and Methods

#### 3.1. Materials

Potassium hydroxide (KOH), potassium persulfate ( $K_2S_2O_8$ ), nickel sulfate hexahydrate ( $NiSO_4 \cdot 6H_2O$ ), copper nitrate gerhardite ( $Cu(NO_3)_2 \cdot 3H_2O$ ), urea ( $CO(NH_2)_2$ ), and ammonium hydroxide ( $NH_3 \cdot H_2O$ ) were purchased from Chongqing Chuandong Co., Ltd. (Chongqing, China). The carbon cloth (type: HCP331N) was obtained from Shanghai Hesen Co., Ltd. (Shanghai, China). All the chemicals were used without further purification.

#### 3.2. Synthesis of Working Electrodes with Catalysts

The carbon cloth was cut into pieces ( $1 \times 2 \text{ cm}^2$ ) as the substrate electrode. The catalysts were grown onto the carbon cloth during the hydrothermal reaction.

Firstly, one piece of the carbon cloth was put into the reaction kettle, and then, the solution with the volume of 40 mL containing 2 mmol metal ions and 150 mg urea was added. The proportion of Ni and Cu is 8:2 if it is not mentioned. The kettle was sealed and heated at  $120 \text{ }^\circ\text{C}$  for 6 h. After cooling to room temperature, the carbon cloth was cleaned by water and named  $NiCu(OH)_2$  in this work.

Then,  $NiCu(OH)_2$  was immersed into 50 mL solution with 1 mol/L KOH and 600 mg  $K_2S_2O_8$ . The solution was heated at  $60 \text{ }^\circ\text{C}$  for 2 h to transform  $NiCu(OH)_2$  into the  $NiCuOOH$  phase. The obtained sample was named  $NiCuOOH-1$ .

The sample treated by a more powerful oxidizing condition was obtained by a similar method with the solution containing 5 mol/L KOH and 1200 mg  $K_2S_2O_8$ . This sample was expected to exhibit a higher crystalline degree of the  $NiCuOOH$  phase, and it was named  $NiCuOOH-2$ .

#### 3.3. Physicochemical Characterization

X-ray diffraction (XRD) patterns were measured on an Ultima IV (Rigaku Corporation, Tokyo, Japan) with the scan rate of  $5^\circ/\text{min}$  and the scan range from  $10^\circ$  to  $90^\circ$ . Scanning electron microscopy (SEM) images were obtained on a Hitachi S-4800 (HITACHI, Tokyo, Japan). Transmission electron microscopy (TEM) images were collected on a JEM F200 (JEOL, Tokyo, Japan) with working voltage of 200 kV. X-ray photoelectron spectra (XPS) were obtained with an ESCALAB 250Xi spectrometer using a nonmonochromatized  $Al K\alpha$  X-ray source (1486.6 eV). The powder of samples was collected from the electrodes for the XRD measurements.

#### 3.4. Electrochemical Measurements and Chemical Analysis

Electrochemical measurements were conducted on CHI660E in a three-electrode cell. The saturated Hg/HgO electrode (SCE) was used as a reference electrode, while a Pt sheet was employed as a counter electrode. The electrochemical measurements were conducted without IR-drop correction. All the samples were activated by cyclic voltammetry (CV) test with the scan rate of  $100 \text{ mV/s}$  in the 1 mol/L KOH solution for more than 20 cycles until the current density is stable. Linear sweep voltammetry (LSV) was performed at the scan rate of  $2 \text{ mV/s}$  in 0.1 mol/L KOH with or without 0.1 mol/L  $NH_3$ . Electrochemical impedance spectroscopy (EIS) was performed in the frequency range of  $0.1\text{--}10^5 \text{ Hz}$  in the solution containing 0.1 mol/L KOH and 0.1 mol/L  $NH_3$ . All the electrochemical measurements were performed at room temperature. A two-chamber reactor divided by a Nafion117 membrane was used in the  $NH_3$  removal experiment to exclude the influence of the counter electrode since the reduction of byproducts on the Pt electrode influences the concentration of both byproducts and  $NH_3$ . The electrode used for the removal of  $NH_3$  is  $5 \text{ cm}^{-2}$ , and the volume of the solution is 50 mL in one chamber. The ammonium was analyzed by Nessler's reagent spectrometry, and the detection wavelength was 420 nm. Nitrite was analyzed by a colorimetric assay under the wavelength of 540 nm according to Chinese national standard method GB 7493-87 [41]. Nitrate was also analyzed by a colorimetric assay according to Chinese national standard method GB 11893-89 [42] with the detection wavelengths of 220 nm and 275 nm. For both nitrite ions and nitrate ions, the samples were

detected three times in parallel using a UV-2550 ultraviolet spectrophotometer (Shimadzu, Tokyo, Japan).

#### 4. Conclusions

In this study, an effective strategy to enhance the activity of NiCu(OH)<sub>2</sub> for the electrochemical oxidation of ammonia by transforming NiCu(OH)<sub>2</sub> into the NiCuOOH phase is provided. By treating NiCu(OH)<sub>2</sub> with an oxidative solution, the partially pre-transformed NiCuOOH electrode presents significantly better performance than NiCu(OH)<sub>2</sub>. Our results indicate that the pre-formation of the NiCuOOH phase can enhance its activity due to the increased number of active sites and the lower charge transfer resistance. However, the sample with a higher crystalline degree of the NiCuOOH phase exhibited lower performance, demonstrating the importance of a moderate treatment condition. Due to the appropriate partial transformation, the optimized NiCuOOH-1 sample presents a high response current density towards ammonia oxidation, low selectivity (<20%) towards NO<sub>2</sub><sup>-</sup>, and stable activity during the long-term operation. This study demonstrated that the pre-formation of the NiCuOOH phase instead of the in situ generation of amorphous NiCuOOH is beneficial for enhancing the performance, which will aid in the development of transition metal catalysts for the electrochemical oxidation of ammonia.

**Supplementary Materials:** The following supporting information can be downloaded at: <https://www.mdpi.com/article/10.3390/molecules29102339/s1>, Figure S1. The XPS survey of NiCu(OH)<sub>2</sub>, NiCuOOH-1 and NiCuOOH-2, respectively. Figure S2. (a) The high-resolution XPS Cu 2p<sub>3/2</sub> spectrum of (a) NiCu(OH)<sub>2</sub> and (b) NiCuOOH-2. Figure S3. The LSVs of NiCu(OH)<sub>2</sub>, with different Ni:Cu ratio in 0.1 mol/L KOH + 0.1mol/L NH<sub>3</sub>. Figure S4. (a) The LSVs of NiCu(OH)<sub>2</sub>, NiCuOOH-1, and NiCuOOH-2 in 0.1 mol/L KOH with or without 0.1 mol/L NH<sub>3</sub>. (b) The Tafel curves calculated from LSVs. Figure S5. (a,b) The SEM images of the NiCuOOH-1 after long-term operation.

**Author Contributions:** Conceptualization, X.Y. and J.Z.; Methodology, X.Y., J.W., J.Z., R.A., R.Z., Y.X., Y.T., Y.L., H.Z. and Y.H.; Writing—original draft, J.Z.; Writing—review & editing, X.Y., J.Z., L.W. and Y.H.; Supervision, J.W., L.W. and Y.H.; Funding acquisition, X.Y. and J.Z. All authors have read and agreed to the published version of the manuscript.

**Funding:** This work was supported by National Natural Science Foundation of China [grant number: 22006005]; Chongqing Municipal Education Commission [grant numbers: KJQN202203214 and KJQN202300838]; Doctor's foundation of Chongqing Industry Polytechnic College [grant number: 2022GZYBSZK3-20]; and Natural Science Foundation of Chongqing [grant number: CSTB2023NSCQ-MSX0700].

**Data Availability Statement:** Data are contained within the article and Supplementary Materials.

**Conflicts of Interest:** Authors Yin Xiong and Yanzong Tao were employed by the company Chongqing Baihan Wastewater Treatment Co., Ltd. The funders had no role in the design of the study; in the collection, analyses, or interpretation of data; in the writing of the manuscript; or in the decision to publish the results.

#### References

1. Zhang, C.; He, D.; Ma, J.; Waite, T.D. Active chlorine mediated ammonia oxidation revisited: Reaction mechanism, kinetic modelling and implications. *Water Res.* **2018**, *145*, 220–230. [CrossRef]
2. Yang, L.; Jiao, Y.; Xu, X.; Pan, Y.; Su, C.; Duan, X.; Sun, H.; Liu, S.; Wang, S.; Shao, Z. Superstructures with Atomic-Level Arranged Perovskite and Oxide Layers for Advanced Oxidation with an Enhanced Non-Free Radical Pathway. *ACS Sustain. Chem. Eng.* **2022**, *10*, 1899–1909. [CrossRef]
3. Xi, X.; Fan, Y.; Zhang, K.; Liu, Y.; Nie, F.; Guan, H.; Wu, J. Carbon-free sustainable energy technology: Electrocatalytic ammonia oxidation reaction. *Chem. Eng. J.* **2022**, *435*, 134818. [CrossRef]
4. Rees, N.V.; Compton, R.G. Carbon-free energy: A review of ammonia- and hydrazine-based electrochemical fuel cells. *Energy Environ. Sci.* **2011**, *4*, 1255. [CrossRef]
5. Tarpeh, W.A.; Barazesh, J.M.; Cath, T.Y.; Nelson, K.L. Electrochemical Stripping to Recover Nitrogen from Source-Separated Urine. *Env. Sci. Technol.* **2018**, *52*, 1453–1460. [CrossRef]
6. Song, J.; Yin Hai, Y.; Jia, Y.; Wang, T.; Wei, J.; Wang, M.; Zhou, S.; Li, Z.; Hou, Y.; Lei, L.; et al. Improved NH<sub>3</sub>-N conversion efficiency to N<sub>2</sub> activated by BDD substrate on NiCu electrocatalysis process. *Sep. Purif. Technol.* **2021**, *276*, 119350. [CrossRef]

7. Zollig, H.; Fritzsche, C.; Morgenroth, E.; Udert, K.M. Direct electrochemical oxidation of ammonia on graphite as a treatment option for stored source-separated urine. *Water Res.* **2015**, *69*, 284–294. [[CrossRef](#)] [[PubMed](#)]
8. Barbosa, J.R.; Leon, M.N.; Fernandes, C.M.; Antoniassi, R.M.; Alves, O.C.; Ponzio, E.A.; Silva, J.C.M. PtSnO<sub>2</sub>/C and Pt/C with preferential (100) orientation: High active electrocatalysts for ammonia electro-oxidation reaction. *Appl. Catal. B Environ.* **2020**, *264*, 118458. [[CrossRef](#)]
9. Liu, H.; Xu, X.; Guan, D.; Shao, Z. Minireview on the Electrocatalytic Ammonia Oxidation Reaction for Hydrogen Production and Sewage Treatment. *Energy Fuels* **2024**, *38*, 919–931. [[CrossRef](#)]
10. Lee, S.A.; Lee, M.G.; Jang, H.W. Catalysts for electrochemical ammonia oxidation: Trend, challenge, and promise. *Sci. China Mater.* **2022**, *65*, 3334–3352. [[CrossRef](#)]
11. Li, S.; Chen, H.; Liu, J.; Deng, Y.; Han, X.; Hu, W.; Zhong, C. Size- and Density-Controllable Fabrication of the Platinum Nanoparticle/ITO Electrode by Pulse Potential Electrodeposition for Ammonia Oxidation. *ACS Appl. Mater. Interfaces* **2017**, *9*, 27765–27772. [[CrossRef](#)] [[PubMed](#)]
12. Ntais, S.; Serov, A.; Andersen, N.I.; Roy, A.J.; Cossar, E.; Allagui, A.; Lu, Z.; Cui, X.; Baranova, E.A.; Atanassov, P. Promotion of Ammonia Electrooxidation on Pt nanoparticles by Nickel Oxide Support. *Electrochim. Acta* **2016**, *222*, 1455–1463. [[CrossRef](#)]
13. Assumpção, M.H.M.T.; Piasentin, R.M.; Hammer, P.; De Souza, R.F.B.; Buzzo, G.S.; Santos, M.C.; Spinacé, E.V.; Neto, A.O.; Silva, J.C.M. Oxidation of ammonia using PtRh/C electrocatalysts: Fuel cell and electrochemical evaluation. *Appl. Catal. B Environ.* **2015**, *174–175*, 136–144. [[CrossRef](#)]
14. Kim, K.-W.; Kim, Y.-J.; Kim, I.-T.; Park, G.-I.; Lee, E.-H. The electrolytic decomposition mechanism of ammonia to nitrogen at an IrO<sub>2</sub> anode. *Electrochim. Acta* **2005**, *50*, 4356–4364. [[CrossRef](#)]
15. Allagui, A.; Sarfraz, S.; Ntais, S.; Al Momani, F.; Baranova, E.A. Electrochemical behavior of ammonia on Ni<sub>98</sub>Pd<sub>2</sub> nano-structured catalyst. *Int. J. Hydrogen Energy* **2014**, *39*, 41–48. [[CrossRef](#)]
16. Zhong, C.; Hu, W.B.; Cheng, Y.F. Recent advances in electrocatalysts for electro-oxidation of ammonia. *J. Mater. Chem. A* **2013**, *1*, 3216–3238. [[CrossRef](#)]
17. Shih, Y.-J.; Huang, Y.-H.; Huang, C.P. In-situ electrochemical formation of nickel oxyhydroxide (NiOOH) on metallic nickel foam electrode for the direct oxidation of ammonia in aqueous solution. *Electrochim. Acta* **2018**, *281*, 410–419. [[CrossRef](#)]
18. Shih, Y.-J.; Huang, Y.-H.; Huang, C.P. Electrocatalytic ammonia oxidation over a nickel foam electrode: Role of Ni(OH)<sub>2</sub>(s)-NiOOH(s) nanocatalysts. *Electrochim. Acta* **2018**, *263*, 261–271. [[CrossRef](#)]
19. Kapalka, A.; Cally, A.; Neodo, S.; Comninellis, C.; Wächter, M.; Udert, K.M. Electrochemical behavior of ammonia at Ni/Ni(OH)<sub>2</sub> electrode. *Electrochem. Commun.* **2010**, *12*, 18–21. [[CrossRef](#)]
20. Siddharth, K.; Chan, Y.; Wang, L.; Shao, M. Ammonia electro-oxidation reaction: Recent development in mechanistic understanding and electrocatalyst design. *Curr. Opin. Electrochem.* **2018**, *9*, 151–157. [[CrossRef](#)]
21. Wang, R.; Liu, H.; Zhang, K.; Zhang, G.; Lan, H.; Qu, J. Ni(II)/Ni(III) redox couple endows Ni foam-supported Ni<sub>2</sub>P with excellent capability for direct ammonia oxidation. *Chem. Eng. J.* **2021**, *404*, 126795. [[CrossRef](#)]
22. Zhang, H.M.; Wang, Y.F.; Kwok, Y.H.; Wu, Z.C.; Xia, H.; Leung, D.Y.C. A Direct Ammonia Microfluidic Fuel Cell using NiCu Nanoparticles Supported on Carbon Nanotubes as an Electrocatalyst. *ChemSusChem* **2018**, *11*, 2889–2897. [[CrossRef](#)] [[PubMed](#)]
23. Xu, W.; Du, D.; Lan, R.; Humphreys, J.; Miller, D.N.; Walker, M.; Wu, Z.; Irvine, J.T.S.; Tao, S. Electrodeposited NiCu bimetal on carbon paper as stable non-noble anode for efficient electrooxidation of ammonia. *Appl. Catal. B Environ.* **2018**, *237*, 1101–1109. [[CrossRef](#)]
24. Xu, W.; Lan, R.; Du, D.; Humphreys, J.; Walker, M.; Wu, Z.; Wang, H.; Tao, S. Directly growing hierarchical nickel-copper hydroxide nanowires on carbon fibre cloth for efficient electrooxidation of ammonia. *Appl. Catal. B Environ.* **2017**, *218*, 470–479. [[CrossRef](#)]
25. Zhu, M.; Yang, Y.; Xi, S.; Diao, C.; Yu, Z.; Lee, W.S.V.; Xue, J. Deciphering NH<sub>3</sub> Adsorption Kinetics in Ternary Ni-Cu-Fe Oxyhydroxide toward Efficient Ammonia Oxidation Reaction. *Small* **2021**, *17*, e2005616. [[CrossRef](#)] [[PubMed](#)]
26. Liu, Z.; Wu, M.; Ma, J. Ni–Cu–Co Grid-like Hydroxyl Oxide Ammonia Oxidation Reaction Catalyst Supported on Carbon Nanotubes. *Energy Fuels* **2022**, *36*, 10339–10345. [[CrossRef](#)]
27. Jiang, X.; Ying, D.; Liu, X.; Liu, M.; Zhou, S.; Guo, C.; Zhao, G.; Wang, Y.; Jia, J. Identification of the role of Cu site in Ni-Cu hydroxide for robust and high selective electrochemical ammonia oxidation to nitrite. *Electrochim. Acta* **2020**, *345*, 136157. [[CrossRef](#)]
28. Zhang, H.; Wang, H.; Zhou, L.; Li, Q.; Yang, X.; Wang, Y.; Zhang, M.; Wu, Z. Efficient and highly selective direct electrochemical oxidation of ammonia to dinitrogen facilitated by NiCu diatomic site catalysts. *Appl. Catal. B Environ.* **2023**, *328*, 122544. [[CrossRef](#)]
29. Nagita, K.; Yuhara, Y.; Fujii, K.; Katayama, Y.; Nakayama, M. Ni- and Cu-co-Intercalated Layered Manganese Oxide for Highly Efficient Electro-Oxidation of Ammonia Selective to Nitrogen. *ACS Appl. Mater. Interfaces* **2021**, *13*, 28098–28107. [[CrossRef](#)]
30. Hao, Y.; Li, J.; Cao, X.; Meng, L.; Wu, J.; Yang, X.; Li, Y.; Liu, Z.; Gong, M. Origin of the Universal Potential-Dependent Organic Oxidation on Nickel Oxyhydroxide. *ACS Catal.* **2023**, *13*, 2916–2927. [[CrossRef](#)]
31. He, S.; Chen, Y.; Wang, M.; Nuomin, H.; Novello, P.; Li, X.; Zhu, S.; Liu, J. Metal nitride nanosheets enable highly efficient electrochemical oxidation of ammonia. *Nano Energy* **2021**, *80*, 105528. [[CrossRef](#)]
32. Huang, J.; Chen, Z.; Cai, J.; Jin, Y.; Wang, T.; Wang, J. Activating copper oxide for stable electrocatalytic ammonia oxidation reaction via in-situ introducing oxygen vacancies. *Nano Res.* **2022**, *15*, 5987–5994. [[CrossRef](#)]

33. Hefnawy, M.A.; Fadlallah, S.A.; El-Sherif, R.M.; Medany, S.S. Synergistic effect of Cu-doped NiO for enhancing urea electrooxidation: Comparative electrochemical and DFT studies. *J. Alloys Compd.* **2022**, *896*, 162857. [CrossRef]
34. Zhou, W.Q.; Xi, B.J.; Chang, X.W.; Wang, B.; Wu, X.Q.; Li, S.; Wu, Y.P.; Li, D.S. Facile in Situ Transformation of NiOOH into MOF-74(Ni)/NiO OH Heterogeneous Composite for Enhancing Electrocatalytic Methanol Oxidation. *Molecules* **2022**, *27*, 2113. [CrossRef]
35. Yoon, J.; Sim, M.; Oh, T.-S.; Yoon, Y.S.; Kim, D.-J. Flexible Electrochemical Sensor Based on NiCu(OOH) for Monitoring Urea in Human Sweat. *J. Electrochem. Soc.* **2021**, *168*, 117510. [CrossRef]
36. Fu, X.-Z.; Zhu, Y.-J.; Xu, Q.-C.; Li, J.; Pan, J.-H.; Xu, J.-Q.; Lin, J.-D.; Liao, D.-W. Nickel oxyhydroxides with various oxidation states prepared by chemical oxidation of spherical  $\beta$ -Ni(OH)<sub>2</sub>. *Solid State Ion.* **2007**, *178*, 987–993. [CrossRef]
37. Zheng, L.; Zhao, Y.; Xu, P.; Lv, Z.; Shi, X.; Zheng, H. Biomass upgrading coupled with H<sub>2</sub> production via a nonprecious and versatile Cu-doped nickel nanotube electrocatalyst. *J. Mater. Chem. A* **2022**, *10*, 10181–10191. [CrossRef]
38. Jiang, K.; Li, K.; Liu, Y.-Q.; Lin, S.; Wang, Z.; Wang, D.; Ye, Y. Nickel-cobalt nitride nanoneedle supported on nickel foam as an efficient electrocatalyst for hydrogen generation from ammonia electrolysis. *Electrochim. Acta* **2022**, *403*, 139700. [CrossRef]
39. El-Nagar, G.A.; Derr, I.; Fetyan, A.; Roth, C. One-pot synthesis of a high performance chitosan-nickel oxyhydroxide nanocomposite for glucose fuel cell and electro-sensing applications. *Appl. Catal. B Environ.* **2017**, *204*, 185–199. [CrossRef]
40. Zhang, M.; Zou, P.; Jeerh, G.; Sun, B.; Walker, M.; Tao, S. Oxygen Vacancy-Rich La<sub>0.5</sub>Sr<sub>1.5</sub>Ni<sub>0.9</sub>Cu<sub>0.1</sub>O<sub>4- $\delta$</sub>  as a High-Performance Bifunctional Catalyst for Symmetric Ammonia Electrolyzer. *Adv. Funct. Mater.* **2022**, *32*, 2204881. [CrossRef]
41. Chinese National Standard Method GB 7493-87. Available online: [https://www.gbstandards.org/GB\\_standard\\_english.asp?code=GB/T%207493-1987](https://www.gbstandards.org/GB_standard_english.asp?code=GB/T%207493-1987) (accessed on 8 May 2024).
42. Chinese National Standard Method GB 11893-89. Available online: <https://www.chinesestandard.net/PDF/English.aspx/GBT11893-1989> (accessed on 8 May 2024).

**Disclaimer/Publisher’s Note:** The statements, opinions and data contained in all publications are solely those of the individual author(s) and contributor(s) and not of MDPI and/or the editor(s). MDPI and/or the editor(s) disclaim responsibility for any injury to people or property resulting from any ideas, methods, instructions or products referred to in the content.